Polytechnic Journal

Polytechnic Journal

Volume 13 | Issue 2 Article 9

November 2023

Lung dosimetry model of inhaled 222Rn for workers at selected building material factories in Erbil City, Iraq

Sardar Qader Othman
Department of Physiotherapy, Erbil Technical Health and Medical College, Erbil Polytechnic University, Kurdistan Region, Iraq., sardarqader@epu.edu.iq

Ali Hassan Ahmed
Department of Physics, College of Science, Salahaddin University-Erbil, Kurdistan Region, Iraq.

Sarbaz Ibrahim Mohammed
Department of Biology, College of Science, Salahaddin University- Erbil, Kurdistan Region, Iraq

How to Cite This Article

Othman, Sardar Qader; Ahmed, Ali Hassan; and Mohammed, Sarbaz Ibrahim (2023) "Lung dosimetry model of inhaled 222Rn for workers at selected building material factories in Erbil City, Iraq," *Polytechnic Journal*: Vol. 13: Iss. 2, Article 9.
DOI: https://doi.org/10.59341/2707-7799.1714

Lung dosimetry model of inhaled 222Rn for workers at selected building material factories in Erbil City, Iraq

Abstract

Radon gas can cause lung harm, leading to extensive research on the biological effects of radon exposure in human lungs under various environmental conditions. The study estimates radon progeny doses for workers in Erbil city's building materials industries, focusing on alpha particle energy deposition, particle clearance, and lung deposition. Using a home condition of 1 Bq.m-3, radon progeny particle-absorbed doses in the trachea, bronchi, bronchioles, alveolar-interstitial sections, and lungs were determined in the first scenario. The 1 Bq.m-3 is replaced with the radon level for each factory to prepare its atmosphere in the second scenario. For the first scenario, the absorbed dose was discovered to be 8.02 in the trachea and bronchi (BB) section, 9.20 in the bronchioles (bb) area, 0.114 in the alveolar-interstitial (AI) section, and 5.78 mGy.WLM-1 in the whole lung. While, for the typical environment of various factories (second scenario), the doses of all regions (BB region, bb region, AI region, and whole lung) ranged from 214.29, 245.82, 3.04, and 154.38 mGy.WLM-1 for workers at the gypsum factory to 1425.39, 1635.11, 20.26, and 1062.92 mGy.WLM-1, respectively, for workers at the red brick 1 factory. In accordance with the scientific literature, the dosimetry method yields a dose conversion factor (DCF) of 13.87 mSv WLM-1 for lung in the first scenario. Advanced dosimetry analysis of breathed radon progeny can reveal structural, biological, and ecological factors affecting absorbed doses and enhance defense against irradiation, especially in high-radon regions.

Keywords

lung dosimetry, radon progeny, absorbed dose, radon concentration

ORIGINAL ARTICLE

Lung Dosimetry Model of Inhaled ^{222}Rn for Workers at Selected Building Material Factories in Erbil City, Iraq

Sardar Qader Othman [a,*], Ali Hassan Ahmed [b], Sarbaz Ibrahim Mohammed [c]

[a] Department of Physiotherapy, Erbil Technical Health and Medical College, Erbil Polytechnic University, Kurdistan Region, Iraq
[b] Department of Physics, College of Science, Salahaddin University, Erbil, Kurdistan Region, Iraq
[c] Department of Biology, College of Science, Salahaddin University, Erbil, Kurdistan Region, Iraq

Abstract

Radon gas can cause lung harm, leading to extensive research on the biological effects of radon exposure in human lungs under various environmental conditions. The study estimates radon progeny doses for workers in Erbil city's building materials industries, focusing on alpha particle energy deposition, particle clearance, and lung deposition. Using a home condition of 1 Bq.m^{-3}, radon progeny particle-absorbed doses in the trachea, bronchi, bronchioles, alveolar-interstitial sections, and lungs were determined in the first scenario. The 1 Bq.m^{-3} is replaced with the radon level for each factory to prepare its atmosphere in the second scenario. For the first scenario, the absorbed dose was discovered to be 8.02 in the trachea and bronchi (BB) section, 9.20 in the bronchioles (bb) area, 0.114 in the alveolar-interstitial (AI) section, and 5.78 mGy.WLM^{-1} in the whole lung. While, for the typical environment of various factories (second scenario), the doses of all regions (BB region, bb region, AI region, and whole lung) ranged from 214.29, 245.82, 3.04, and 154.38 mGy.WLM^{-1} for workers at the gypsum factory to 1425.39, 1635.11, 20.26, and 1062.92 mGy.WLM^{-1}, respectively, for workers at the red brick 1 factory. In accordance with the scientific literature, the dosimetry method yields a dose conversion factor (DCF) of 13.87 mSv WLM^{-1} for lung in the first scenario. Advanced dosimetry analysis of breathed radon progeny can reveal structural, biological, and ecological factors affecting absorbed doses and enhance defense against irradiation, especially in high-radon regions.

Keywords: Lung dosimetry, Radon progeny, Absorbed dose, Radon concentration

1. Introduction

Many epidemiological investigations and animal testing have indicated that contact with radon (^{222}Rn) is related to pulmonary disease [1–3]. This is expected because alpha particles that are emitted by radon daughter are coated on the membranes of pulmonaria's passageways and may directly displace atomic structures, resulting in chemical and biological alterations when absorbed by sensitive cells. During the radiolysis of water, it can also indirectly intervene. Also, several studies have been performed not just on humans [4] but also on animals used in research [5–8].

Radon is a chemically inert gas that is colorless, odorless, and tasteless. Naturally, it originates from soil, building materials, and water [9]. It is created when radium, a byproduct of uranium decay, is released. The general populace's interior exposure to radon and its offspring has been reported to have a dangerous dose effect. The majority of natural public exposure comes from radon and its rapidly decomposing byproducts, which account for around 50% of the effective population dose globally [10]. After smoking tobacco, radon is the second-biggest cause of lung cancer. The hazards caused by inhaling radon decay products are lung cancer, skin cancer, and kidney diseases [11]. Inhaled radon

Received 15 July 2023; accepted 7 September 2023.
Available online 1 December 2023

* Corresponding author.
E-mail addresses: sardarqader@epu.edu.iq (S.Q. Othman), ali.ahmed@su.edu.krd (A.H. Ahmed), sarbaz.mohammed@su.edu.krd (S.I. Mohammed).

https://doi.org/10.59341/2707-7799.1714

typically remains in or is discharged from the lung airways unharmed because it is an inert gas. Nonetheless, the bloodstream may retain 1% of the radon inhaled through gas exchange and distribute it throughout the flesh [12,13]. This implies that in addition to exposing the lungs, radon could harm a variety of structures and systems; however, the radiation doses that result are significantly lower than those that arise from radon progeny inhalation. Dose conversion factors for radon, such as for uranium miners, have been found by comparing the danger per unit dose from sources other than radon research, such as atomic bomb survivors, to the danger per unit contact in the working level month (WLM) from radon analyses. Epidemiology-based dose conversion factors are known, and they are frequently stated as an effective dose per unit exposure ($mSv.WLM^{-1}$). It's crucial to keep in mind that the risk of dying from lung cancer might be comparable to the radon health risk [14]. The International Commission for Radiological Protection (ICRP) updates and publishes the risk thresholds for inhaling radon on a regular basis [15]. The Committee provided figures for the risk of lung malignancy demise for staffs and the overall civic (as well as kids) of 5.6×10^{-5} and 7.3×10^{-5} mSv^{-1}, respectively. These numbers were later changed to 4.2×10^{-5} and 5.7×10^{-5} mSv^{-1} [16], depending on the old values [15,17]. For the population and the employees, the rounded dose conversion factors for radon were 4 and 5 $mSv.WLM^{-1}$, respectively. The updated risk scores, though, produce dose conversion factors of 9 and 12 $mSv.WLM^{-1}$ [16,18].

There have been some epidemiological investigations to see whether there is a connection between radon gas and leukemia since it can more easily be disseminated into the red bone marrow [19,20]. Also, mice were exposed to radon gas in certain experiments on animals at different doses and for different lengths of time [21]. In these situations, precisely estimating the absorbed doses for the relevant human organs or tissues would enable a quantitative discussion of biological reactions. The objective of the current research is to estimate absorbed doses in workers lungs at selected building material factories in Erbil City arising from radon progeny inhalation. The outcomes will be compared to those from other mathematical models.

2. Material and methods

2.1. The study area

Based on the past studies, indoor radon levels in a few enterprises producing building supplies in Erbil, the regional capital of Iraqi Kurdistan, were monitored. Over 1.9 million people live in Erbil, which covers an area of 80,000 square kilometers. The average radon concentration readings varied from 26.72 to 177.73 $Bq.m^{-3}$ [22]. The annual effective dose was determined to be (2.179 1) $mSv.y^{-1}$ on average, and the annual lung cancer rate per 10^6 people was reported to be (94.125) [22]. The location and the measured average radon concentration in the study area were illustrated as shown in Figure 1 and Table 1.

To determine the lung dose of radon that workers in the factories inhaled, the current study has adopted two scenarios. The first scenario was chosen as a home condition with 1 $Bq.m^{-3}$ of radon concentration, and the second scenario is based on the selected building material factories environment from previous work [22] with an average radon concentration ranging from (26.72–177.73) $Bq.m^{-3}$. In this study, male participant utilized the mathematical lung model adopted by [23]. Using lungs with completely expanded volumes, the initial model was created (i.e., TLC). To accommodate the lung volume of interest, which is the lung volume during both the inspiratory and expiratory segments, the pulmonary artery dimensions have been reduced [24]. As displayed in Table 2 for humans, there are 25 phases in the pulmonary model. The tracheobronchial (TB) and alveolar-interstitial (AI) sections are two different categories for airflow generation. The trachea and bronchi (BB area), the bronchioles, and the terminal bronchioles are additional divisions of the TB region (bb region). The interfacial connective tissues, alveolar ducts, and respiratory bronchioles make up the AI area. The Human Respiratory Tract Model (HRTM), created by the International Commission on Radiological Protection, is congruent with this designation [25].

Table 3 summarizes physiological parameters associated with breathing. A worker who uses their nose to breathe was used to establish the breathing parameters for humans while performing light duty (68.75% bright workout and 31.25% sedentary break) [25]. The TLC corresponds to the original size of the employed pulmonary models and is the total volume of all airways in the lungs when wholly extended has been used [26,27]. Regarding particles, the following presumptions were applied: Aerosol particles have a density of 1 g cm^3 and are oval. Because aerosols have a dimensionless, highly porous growth factor, they do not collect water and do not vary in size as they travel through the lung air passages.

At a radon concentration of 1 $Bq.m^{-3}$, the ratios of ambient radioactive concentrations were first supplied as a function of doses to the trachea and

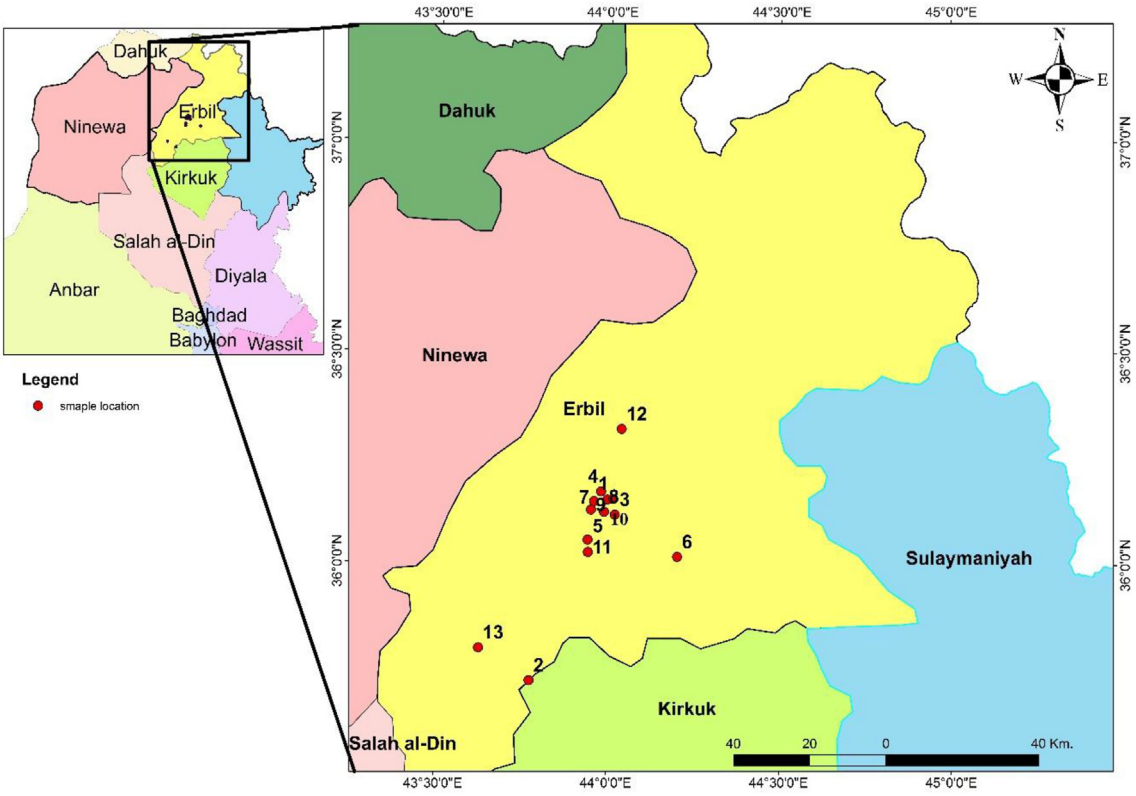

Figure 1. The locations surveyed for this study [22].

bronchi, bronchioles and terminal bronchioles, alveolar-interstitial regions, and total lungs. The ratios are ^{222}Rn: ^{218}Po: ^{214}Pb: ^{214}Bi: ^{214}Po = 1:0.84: 0.45:0.2:0.2 for radon progeny attached to aerosols and 1:0.026:0.0026:0:0 for those unattached. This corresponds to F = 0.4 and f_p = 0.06, which reflect the ambient settings in homes [14,24,29].

2.2. Particle deposition

Following that, particle depositions for air passageway divisions in the BB, bb, and AI regions were identified. Particle diffusion was one of the theorized deposition mechanisms used in the computations, along with sedimentation or internal impaction [24], as given below.

Table 1. Radon activity concentration in the studied factories (Bq.m^{-3}) [22].

No.	Factory	Radon activity concentration (Bq.m^{-3})
1	Artificial-marble	38.31
2	Cement-plant	127.37
3	Lightweight block	107.81
4	Marble	113.44
5	Red-brick 1	177.73
6	Red-brick 2	169.46
7	Concrete-block1	51.46
8	Concrete-block 2	54.46
9	Crusher-stone	87.50
10	Kashi-mosaic	58.30
11	Tile	64.09
12	Ceramic	46.06
13	Gypsum	26.72

2.2.1. Diffusion [24]

$$\eta_{i,D} = 1 - 0.819e^{-7.314xi} - 0.0976e^{-44.61xi} - 0.0325e^{-114xi} - 0.0509e^{-79.31xi^{2/3}} \quad (1)$$

$$\text{For laminal flow } \eta_{i,D} = 2.828X^{\frac{1}{2}}\left(1 - 0.314X^{\frac{1}{2}} + \ldots\right) \quad (2)$$

$$\text{For turbulent flow } \eta_{i,D}^{E} = 1 - (1 - \eta_{i,D})^{f_e} \text{ for } 10 < \frac{L_i}{R_i} \quad (3)$$

$$x = \frac{L_i D_P}{2R_i^2 \overline{v}_i} \quad (4)$$

where D_p is the particle-air diffusion coefficient in $cm^2.s^1$. The diffusion coefficient for the aerosol particle can be derived from the Stokes–Einstein equation [30].

Table 2. Characteristic pulmonary models for humans [23,24].

Region	Subregion	Generation	n_i	$L_i(mm)$	$D_i(cm)$	$\theta_i(^\circ)$	$\varnothing_i(^\circ)$	$V_i(cm^3)$	$S_i(cm^2)$	$\bar{v}_i(mm.sec^{-1})$	$m_T(Kg)$
TB	BB	1	1	100	2.01	0	0	31.73	3.17	1191.23	0.000158
		2	2	43.6	1.56	33	20	16.67	3.82	988.8	0.000107
		3	4	17.8	1.13	34	31	7.14	4.01	942.26	0.000634
		4	8	9.65	0.827	22	43	4.15	4.3	879.6	0.000505
		5	16	9.95	0.651	20	39	5.3	5.33	709.75	0.000821
		6	32	10.1	0.574	18	39	8.36	8.28	456.46	0.000147
		7	64	8.9	0.435	19	40	8.47	9.51	397.4	0.000198
		8	128	9.62	0.373	22	36	13.46	13.99	270.25	0.000368
		9	256	8.67	0.322	28	39	18.07	20.85	181.31	0.000574
	bb	10	512	6.67	0.257	22	45	17.72	26.56	142.31	0.000185
		11	1024	5.56	0.198	33	43	17.53	31.53	119.88	0.000239
		12	2048	4.46	0.156	34	45	17.46	39.14	96.56	0.000304
		13	4096	3.59	0.118	37	45	16.08	44.79	84.38	0.000372
		14	8192	2.75	0.092	39	60	14.98	54.46	69.41	0.000448
		15	16,384	2.12	0.073	39	60	14.54	68.57	55.11	0.000553
		16	32,768	1.68	0.06	51	60	15.57	92.65	40.8	0.000728
AI		17	65,536	1.07	0.054	45	60	20.11	150.09	26.03	0.00011
		18	131,072	0.96	0.05	45	60	30.88	257.36	15.18	
		19	262,144	0.74	0.047	45	60	41.84	454.81	8.6	
		20	524,288	0.64	0.045	45	60	66.71	833.84	4.68	
		21	1,048,576	0.56	0.044	45	60	111.61	1594.39	2.45	
		22	2,097,152	0.5	0.044	45	60	200.89	3188.78	1.23	
		23	4,194,304	0.46	0.043	45	60	347.19	6090.97	0.63	
		24	8,388,608	0.42	0.043	45	60	645.64	12181.95	0.31	
		25	3*108	0.2	0.03	45	60	3871.8	–	0.018	

Where n_i is the number of passageways in the i^{th} iteration
D_i is the pulmonary diameter in the i^{th} generation (cm).
$\bar{v}_i$ represents air's average flow rate during intake or exhaust in the ith generation ($mm.sec^{-1}$).
L_i is the pulmonary distance in the i^{th} generation (cm).
θ_i is the shift in bulk air movement direction from the i - 1^{th} section into the i^{th} section, which is represented by the branched angle (rad).
$\varnothing_i$ is the i^{th} generation's inclination angle (rad).
V_i is the nasal capacity in the i.t. generation (cm^3).
S_i is the average circumference of the ith group's passageways (cm^2).
m_T is the target weight (kg).

$$D_P = \frac{k_B T}{3\pi\mu d_p} \tag{5}$$

Where k_B is the Boltzmann constant, which equals $1.38*10^{-16}$ gm $cm^2.s^{-2}$. k^{-1}, T is the room temperature (293 K), μ is the viscosity of air at normal temperature ($1.81*10^{-4}$ $g.cm^{-1}$. s^{-1}) and d_p is the particle diameter (200 nm for attached particles and 1 nm for unattached particles) [28].

R_i represents the pulmonary radius in the ith generation (cm).

$\bar{v}_i$ is the air's average flow rate during intake or exhaust in the ith generation ($cm.s^{-1}$).

For the effect of entrance configuration

$$f_e = 1 + \left(\frac{2\theta_i}{\pi}\right)\left(13 - \frac{12\theta_i}{\pi}\right)\left(\frac{2R_i}{L_i}\right) \tag{6}$$

2.2.2. Sedimentation [31]

$$\eta_{i,s} = 1 - \exp\left(\frac{-4gC\rho_p r_p^2 L_i \cos\varnothing_i}{9\pi\mu R_i \bar{v}_i}\right) \tag{7}$$

Where

Table 3. Physiological parameters for humans [24,28].

Class	TLC (ml)	TV (ml)	LV (ml)	FRC (ml)	f (min^{-1})	B ($ml.min^{-1}$)
Humans	6993.52	1094	3847	3300	17.5	20,000

TLC: Total lung capability (ml), or the amount of air that can be taken in by the lungs at their full potential.
TV: Tidal volume (ml), which measures the amount of air taken in and expelled during an inhalation.
LV: Altering lung capacity (ml).
FRC: Capacity for functioning residuals (ml), which is the amount of air in the lungs at the end of a typical gasp.
F: Breathing frequency (min^{-1}).
B: The rate of breathing ($ml.min^{-1}$).

$$C = \frac{1}{1 + 0.42 \times K_n} + 1.67K_n \text{ and } K_n = \frac{\lambda_p}{r_p} \quad (8)$$

$$\lambda_p = \frac{KT}{\sqrt{2}\,\pi d_p^2 P} \quad (9)$$

where C is the Cunningham slip correction factor, g is the acceleration due to gravity (cm.s^{-2}), ρ_p is the particle density (kg.cm^{-3}), r_p represents the particle radius (cm), μ is the air's viscosity (kg.cm^{-1}.s^{-1}), K_n is the Knudsen number, λ_p is the mean free route of airborne molecules (cm), and P is the pressure at 1 atmp (1 atmp = 760 and Tor = 760 mmHg).

2.2.3. Internal impaction [24]

$$\eta_{i,I} = 1 - \frac{2}{\pi}\cos^{-1}(\theta_i.S_{tK}) + \frac{1}{\pi}\sin\{2\cos^{-1}(\theta_i.S_{tK})\} \quad (10)$$

For $\theta_i.S_{tK} < 1$ *and* $\eta_{i,D} = 1$ for $1 \le \theta_i.S_{tK}$

Where S_{tK} is the number of stokes given in the following equation:

$$S_{tK} = \frac{C\rho_P r_p^2 \overline{v}_i}{9\mu R_i} \quad (11)$$

The following equation can be used to determine the overall efficiency of every step [32]:

$$\eta_i = \eta_{i,D}^E + \eta_{i,s} + \eta_{i,I} - \eta_{i,D}^E\eta_{i,s} - \eta_{i,D}^E\eta_{i,I} - \eta_{i,s}\eta_{i,I} + \eta_{i,D}^E\eta_{i,s}\eta_{i,I} \quad (12)$$

The deposition fraction must be calculated after obtaining the deposition efficiency; this is distinct from the deposition efficiency. The portion of gasped particles that is accumulated in successive generations of the airways throughout a sniff is known as the deposition fraction. It is calculated using the cubicle model described in [33]. The respiratory system is viewed in this framework as a system made up of numerous partitions (i.e., airway stages) that are sequentially linked (Figure 2).

The air that is inhaled can be split up into different parts, and each of them approaches a specific generation throughout inhalation. The following link exists between the tidal volume and airway volumes:

$$TV = V1 + V2 + V3 + \ldots + V_L \quad (13)$$

The final compartment that the inhaled air reaches is the VL. The air breathed does not reach the 25th generation of rats because Generation L

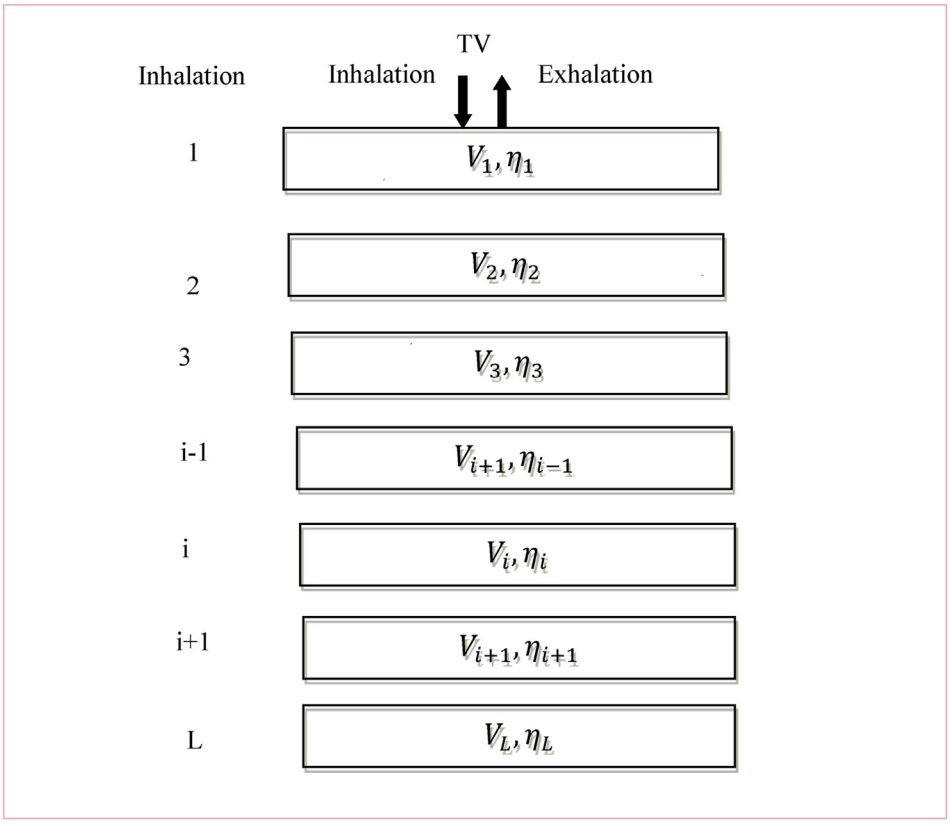

Figure 2. Compartment method for estimating proportions of particles deposited [24].

was 24 for them. It should be emphasized that this equation makes no assumptions regarding the mixing of residual air and inhaled air. Upon inhalation, the deposition portion in the ith cubicle can be represented as [24,33].

$$DE_{i,In} = (1-\eta_{1,In})(1-\eta_{2,I,n})\ldots(1-\eta_{i-1,In}) \times \{\eta_{i,In}(V_{i+1}+V_{i+2}+\ldots+V_L)+0.5\eta_{i,In}V_i\}\left(\frac{1}{TV}\right) \quad (14)$$

Additionally, the following formula can be used to determine the deposition fraction during exhalation:

$$DE_{i,Ex} = \left[\prod_{j=1}^{i-1}(1-\eta_{j,In})\right](1-0.5\eta_{i,In})0.5\eta_{i,Ex}\frac{V_i}{TV} + \left[\prod_{j=1}^{i}(1-\eta_{j,In})\right]\eta_{i,Ex} \times \sum_{j=i+1}^{L}\left[\prod_{K=i+1}^{j-1}(1-\eta_{k,Ex})(1-\eta_{k,In})\right] (1-0.5\eta_{j,In}) \times (1-0.5\eta_{j,Ex})\left(\frac{V_j}{TV}\right) \quad (15)$$

The total deposition fraction (DE_i) per breath is calculated as the product of $DE_{i,In}$ and $DE_{i,Ex}$. The sum of DEi over all compartments was used to compute the particle depositions for BB, bb, and AI [24,33].

2.3. Particle clearance model

There are three primary methods to eliminate particles trapped in the respiratory system: (a) the mucociliary enters the digestive system and transports them to the pharynx; (b) lymphatic vessels enter local lymph nodes; and (c) the particles are broken down and metabolized in the bloodstream. Only the mucociliary activity in the BB and bb areas was included in the clearance design in the current investigation. This is because processes (b) and (c) typically proceed at rates that are substantially slower than processes (a) and the rates at which radon daughters' decay. The current analysis does not take into account any clearances in the AI region [28,30,34,35].

Table 4 includes a table of the mucous velocity characteristics for each duct secretion in the BB and bb areas. The velocities v_i *mm* .$\min^{-1}$ were assessed by Eq (16). From [34].

$$v_i = \frac{v_1 D_1}{n_i D_i} \quad (16)$$

Table 4. Criteria for mucociliary clearance in humans [24].

Region	Subregion	Generation	For humans	
			$v_i(mm.min^{-1})$	$\overline{T}_i(min)$
TB	BB	1	5.5	9.1
		2	4	5.5
		3	2	4.5
		4	1.3	3.7
		5	1	5.0
		6	0.9	5.6
		7	0.7	6.4
		8	0.6	8.0
		9	0.4	10.8
	Bb	10	0.3	11.1
		11	0.2	13.9
		12	0.1	22.3
		13	0.04	44.9
		14	0.02	68.8
		15	0.005	212.0
		16	0.001	840.0

The mucous speed of the trachea can be used to compute the velocities for the remaining divisions (generation 1). The velocity in the trachea, v_1 *mm*.$\min^{-1}$, might be roughly calculated using the weight W (kg) from [36].

$$v_1 = 3.02W^{0.41} \quad (17)$$

where n_i number of airways in the ith section, D_1 is the tracheal diameter, and D_i is the airway diameter in the ith generation (mm).

The mean residence time $\overline{T}_i(min)$ of particles within every airway iteration was then determined from the equation below.

$$\overline{T}_i = \frac{0.5L_i}{v_i} \quad (18)$$

The values of $\overline{T}_i$ appear to be equivalent to the half-lives of radon progeny, with short half-lives 3.10 min for ^{218}Po, 26.8 min for ^{214}Pb, 19.9 min for ^{214}Bi, and 164.3 μmin for ^{214}Po).

Using [34], who employed a compartmentalized model with series connections between the airflow segments, the principal equations describing the kinetics of particle clearance were derived. This allows us to express the variation in the number of radon descendants in the ith phase per time as [24]:

$$\frac{dM_{i,po-218}}{dt} = DE_{i,po-218}.B.N_{PO-218} - \frac{M_{i,po-218}}{\overline{T}_I} + \frac{M_{i+1,PO-218}}{\overline{T}_{i+1}} - M_{i,po-218}\lambda_{po-218} \quad (19)$$

$$\frac{dM_{i,pb-214}}{dt} = DE_{i,pb-214}.B.N_{Pb-214} - \frac{M_{i,pb-214}}{\overline{T}_I} + \frac{M_{i+1,Pb-214}}{\overline{T}_{i+1}} - M_{i,pb-214}\lambda_{pb-214} + M_{i,po-218}\lambda_{po-218} \quad (20)$$

$$\frac{dM_{i,Bi-214}}{dt} = DE_{i,Bi-214}.B.N_{Bi-214} - \frac{M_{i,Bi-214}}{\overline{T}_I} + \frac{M_{i+1,Bi-214}}{\overline{T}_{i+1}} - M_{i,Bi-214}\lambda_{Bi-214} + M_{i,pb-214}\lambda_{pb-214} \quad (21)$$

All generations of the differential equation set in the BB and bb areas were quantitatively determined. Using the decay constants of lambda λ_n, the solutions of $M_{i,n}$ were merely translated to the radioactivity of $A_{i,n}$. Due to radiological equilibrium, it is fair to infer that $A_{i,po-214}$ is equal to $A_{i,Bi-214}$ in these circumstances.

$$\lambda_n = \frac{ln\,2}{t_{1/2}} = \frac{0.693}{t_{1/2}} \quad (22)$$

λ_n is the decay constant (min^{-1}), and n denotes a radioisotope in the suffix.

$M_{i,n}$ is the number of particles implanted in the ith generation. A particle is a radioisotope, which is what the suffix n" stands for.

2.4. Dosimetry

Calculations were made to determine the average energy absorbed in the targeting (T) per radiation emitted from the supply (S); this is known as the absorbing fraction (AF). reference [24] which provides the AF.

$$AF(T \leftarrow S)_R = \frac{E(T \leftarrow S)_R}{E_R} \quad (23)$$

where $E(T \leftarrow S)_R$ is the radiation energy and E_R is the typical amount of energy that T receives for each release of R in S. Because beta particles and gamma rays have far lower absorbed energy than alpha particles, only alpha particles from ^{218}Po and ^{214}Po are taken into account in this AF computation. The absorption of those alpha particles from mucus tissue (the source) to several goal tissues was measured [24].

The dose that was absorbed, D_T (Gy), can be computed as follows:

$$D_T = \frac{1.6 \times 10^{-13} \times A_i E_\alpha AF(T \leftarrow S)_\alpha}{m_T} \quad (24)$$

where A_i (Bq) is the radioactivity in the ith section, E_α (MeV) is the alpha particles' fundamental energy, and m_T (kg) is the target weight.

Each generation's absorbed dose in the region was evenly summed to acquire $D_{BB}(= 0.5\,D_{secretory} + 0.5\,D_{basal})$, D_{bb}, or D_{AI}, respectively. The dose of the entire lung (DWL) was subsequently computed as follows [28].

$$D_{WL} = \frac{1}{3}(D_{BB} + D_{bb} + D_{AI}) \quad (25)$$

Equation (26) gives the effective dose of radon progeny nuclide-induced lung (in Sv. Bq^{-1}).

$$E = W_T \times W_R \times D_{WL} \quad (26)$$

Where $W_T = 0.12$ denotes the lung's tissue weighting factor. Moreover, $W_R = 20$ stands for the particle's radiation weighting factor [37].

3. Results and discussion

The homogeneity of the absorbing fraction (AF) of alpha particles released from radon daughters in the mucus is depicted in Figure 3. The AFs at various places have differing strengths depending on the various target categories. Even though the geometry of the source and the target is different in this article, the absorbing fraction results presented here are comparable to those of the radon daughter presented in [24]. This outcome could be interpreted qualitatively by considering the distribution of alpha particles and the separation of the supplier and the objective. In the BB section, take into account the AF of ^{218}Po for secretory tissues, as shown in Figure 3a. The ranges of ^{214}Po (7.69 MeV) and ^{218}Po (6.00 MeV) alpha particles in water are approximately 50 and 74 μm, respectively. For humans, the separation between the secretory tissue and the mucus is about 50 μm. The peak of an alpha particle's stopping power occurs right before the range's end. As a result, the absorbing fraction tends to increase when the separation across the source and the objective approaches the alpha particle's effective range. This also explains the striking differences in AFs between the BB and bb sections revealed in Figure 3. For instance, in the BB and bb areas of humans, the close proximity of the mucus to the secretory tissue is around 50 and 20 μm, respectively. This distance for the BB region is comparable to the alpha particle range (50 or 74 μm), so it is predicted that the energies will be absorbed more efficiently in the BB region by the target layer than in the bb region [24,25].

For both scenarios, rates of absorbed doses were calculated using particle deposition and

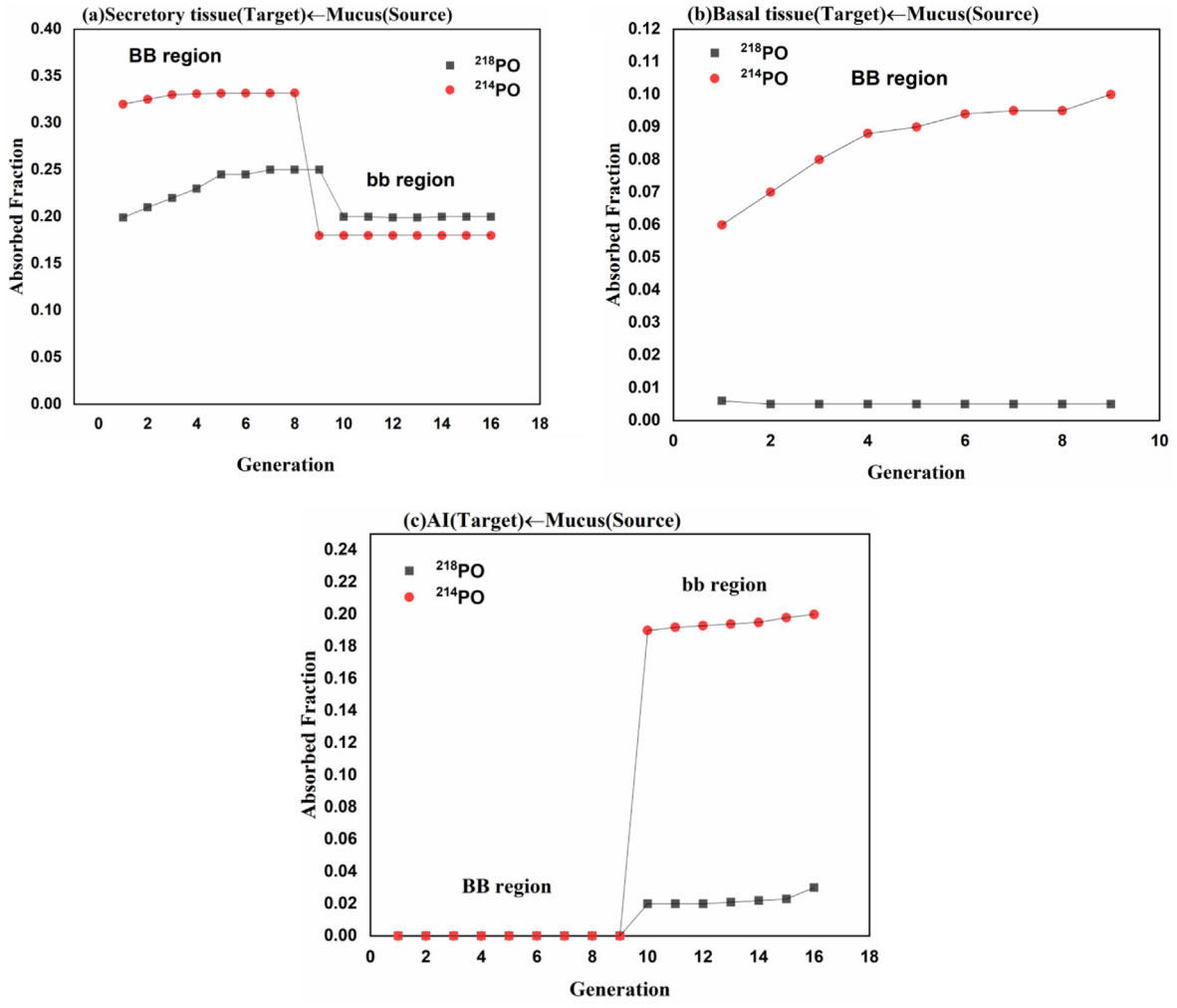

Figure 3. Absorbing fractions (AF) of alpha particles of ^{218}Po and ^{214}Po for different generation and regions [24].

clearance models. The complete lung and each region's absorbed doses are displayed in Table [5]. The definition of a reference home environment condition, which is nearly identical to [14,28], was provided in the first scenario as shown in Table 3. This is consistent with the average atmospheric conditions in dwellings: F = 0.4 (equilibrium factor) and fp = 0.06 (unattached fraction). The second scenario, though, came from atmospheric conditions in the selected building factories previously reported by [22]. The only thing that changed was the radon concentration at each factory. The result shown in Table 5 is that the bb and BB regions have the highest absorbed dose compared to the AI region. Because the specific tissues in the BB and bb areas have lesser masses than those in the AI region, the doses to the bronchial (BB) and bronchiolar (bb) regions are higher than those to the alveolar-interstitial (AI) region [38].

Due to the high dose of radon inhaled through the bronchi, Figure 3 demonstrates that BB areas had the highest absorbed dose. This was due to the deposition of radon decay products or their progeny, which emit alpha radiation into the bronchi and lungs, thereby increasing the risk of lung cancer [39].

Absorbed doses of lungs were compared for two dissimilar scenarios of radon and its byproducts exposure. Radon gas is the source of exposure in cases 1 and 2, and its degradation products (^{218}Po and ^{214}Po) also contribute to the doses. This is because ^{218}Po has a half-life of 3.05 min and is the direct progeny arising from the decay of ^{222}Rn. When ^{218}Po decays, it emits α-particle with a relatively high energy of 6.12 MeV. The absorbed doses calculated in the first scenario in all regions (D_{BB}, D_{bb}, $D_{AI,}$ and whole lung) are 8.02, 9.2, 0.114 and 5.78 mGy.WLM^{-1}, respectively, which is in agreement with that made by [38]. Table 6 demonstrates

Table 5. Absorbed doses of the BB, bb, and AI regions in addition to the whole lung doses for workers resulting from exposure to radon progeny.

Absorbed dose (mGy.WLM^{-1})					Effective dose (mSv. WLM^{-1})
Regions	BB region	bb region	AI region	Whole lung	
Scenario 1	8.02	9.20	0.114	5.78	13.87
Scenario 2					
Artificial-Marble	307.25	352.45	4.36	221.35	531.24
Cement-Plant	1021.05	1171.80	14.52	735.79	1765.89
Lightweight-Block	864.63	991.85	12.29	622.92	1495.00
Marble	909.78	1043.64	12.93	655.45	1573.08
Red-Brick 1	1425.39	1635.11	20.26	1026.92	2464.60
Red-Brick 2	1359.07	1559.03	19.32	979.14	2349.94
Concrete-Block1	412.71	473.43	5.87	297.33	713.59
Concrete-Block 2	436.77	501.03	6.21	314.67	755.21
Crusher-Stone	701.75	805.00	9.97	505.57	1213.37
Kashi-Mosaic	467.57	536.36	6.64	336.84	808.42
Tile	514.00	589.63	7.31	370.31	888.74
Ceramic	369.40	423.75	5.25	266.13	638.71
Gypsum	214.29	245.82	3.04	154.38	370.51

Table 6. Comparing the amounts of radiation that are regionally absorbed by the workers' lungs at home (mGy.WLM^{-1}).

Tissue target	Present work	[38]	[14]	[28]	[40]
BB	8.02	8.9	5.4	6.28	5.9
Bb	9.2	9.2	4.72	5.84	2.65
Al	0.114	0.33	0.19	0.2	0.15
Whole lung	5.78	6.14	3.44	4.11	3.2

that the outcomes of [14,28,40] are generally inferior to those of this work. This could be due to the fact that the input parameters and models used in various works are distinct. Winkler-Heil et al., claim that the geometric model of the respiratory tract has less impact on the absorbed dose rate than factors like breathing rate, radon progeny particle size, and unattached fraction [40].

According to Table 5, the lung's absorbed dose in the atmosphere within the house is 5.78 mGy. WLM^{-1}. It is possible to calculate the lung's effective dose, also referred to as the dose conversion factor (DCF), by multiplying the absorbed doses by the lung's tissue weighting factor and the particle weighting factor. The result is 13.87 mSv. WLM^{-1}. As shown in Table 7, this outcome is comparable to

Table 7. Literature-reported dose conversion factor (DCF) per unit consumption for radon daughters.

DCF (mSv. WLM^{-1})	Reference
15	[38]
13	[42]
15	[43]
9.86	[28]
8.25	[14]
21.1	[41]
8	[44]
7.6	[45]
10–16	[46–48]
13.87	**Present work**

the DCFs found in previous publications. Despite this, the effective dose reported by [41] is significantly higher than that of other results, which may be due to the fact that the particle size they employed was significantly different from that used in other research studies. The obtained DCF is comparable to the findings of [38,42,43]. The DCF achieved in the current study using the respiratory tract model and the T-B tree's successive generations is within the acceptable bounds of the findings published in other papers as shown in Table 7. The most recent DCF levels based on epidemiological studies are 9 mSv WLM^{-1} for the general population and 12 mSv WLM^{-1} for employees. Evidently, the current DCF value of 13.87 mSv. WLM^{-1} and the value obtained from epidemiological data are very similar.

For the second scenario, the same parameters as the first scenario have been used for a group of selected construction materials in Erbil city, that have been mentioned in Table 2. In the second scenario, the radon level of each factory, as shown in Tables 1 and is set instead of 1 Bq.m^{-3} to prepare the factories atmospheric condition. The absorbed dose for the second scenario at selected building ingredient factories for the regions BB, bb, AI, and the whole lung ranged from 214.29, 245.82, 3.04, and 154.38 mGy.WLM^{-1} for workers at the gypsum factory to 1425.39, 1635.11, 20.26, and 1062.92 mGy.WLM^{-1}, respectively, for workers at the red brick 1 factory. The results shown in Table 5 indicate that the doses in all regions increased by a factor of 10^3 during the transition from the first scenario to the second scenario of the radon atmosphere. Notwithstanding the fact that equation (24) was obtained by calculations for the absorbed dose, it can roughly reflect this increment. This implies

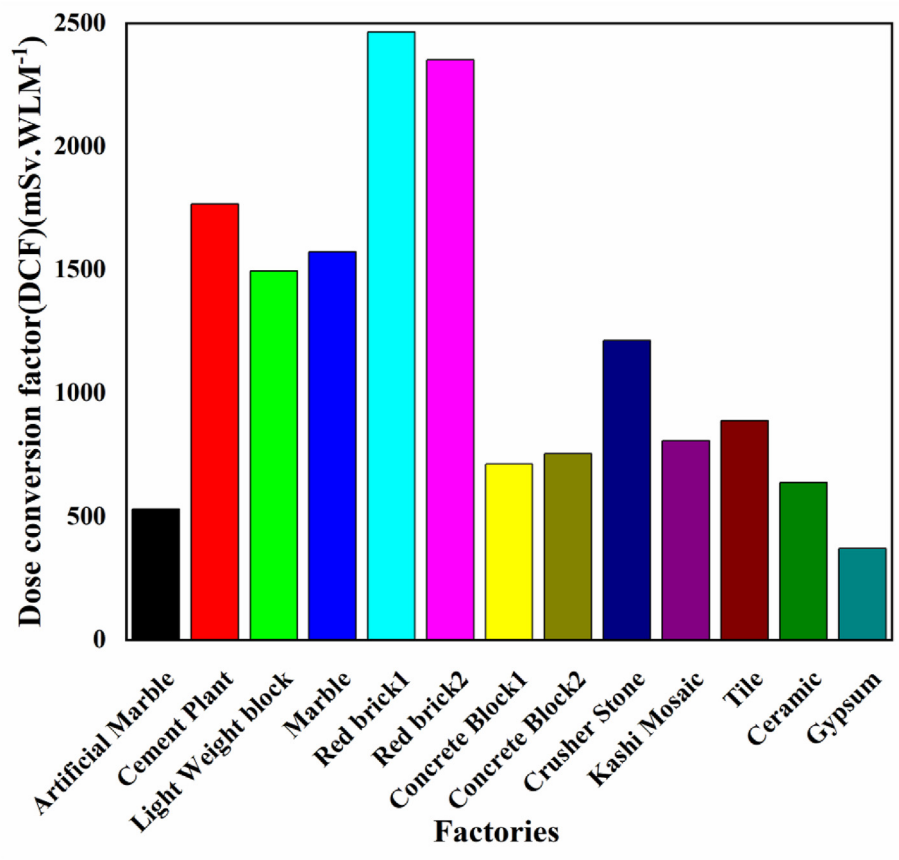

Figure 4. Dose conversion factor (DCF) for the different investigated factories in Erbil city.

that the radon concentration is one of the crucial factors affecting the dose. For the second scenario, the red brick1 factory had the highest effective dose of 2464.60 mSv. WLM^{-1}, while the lowest value was equal to 370.51 mSv. WLM^{-1} for the gypsum factory, as shown in Figure 4. These results indicate that the high levels of radon play a significant role in the determination of the effective dose for workers in various environmental conditions. The reason behind that refers to more radon gas inhalation from the dust yields during the crushing and powdering processes of building material preparation for workers in this field [49]. When compared to other manufacturers, the results also revealed a considerable disparity, particularly among those producing concrete blocks, gypsum, ceramics, and artificial marble. Doors and windows in gypsum and concrete block manufacturers are usually largely left unlocked throughout the day, which aids in the movement of heat from inside to outside, causing radon to drift to the outside and reducing the quantity of radon that workers ingest. The majority of air exchange methods in these locations involve air conditioning, which raises the threshold for ambient humidity and aids in the movement of radon gas. This may be associated the maximum value of an effective dose in other enterprises. As a result, compared to other factories, the workers at those are exposed to higher levels of radon annually [22]. It is concluded from the discussion above that the dose estimation for humans from radon products that are swallowed, as performed in the current study, yields credible consequences.

4. Conclusion

Many models for math, ranging from particle deposition to dosimetry, were illustrated for predicting the pulmonary doses of radon progeny in humans. Following that, lung doses from inhaling radon progenies were supplied for a C_{Rn} of 1 $Bq.m^{-3}$, which helps predict doses in varied environmental situations. For the first scenario, the absorbed dose was found to be 8.02 $mGy.WLM^{-1}$ in the area of trachea and bronchi (BB) section, 9.20 mGy WLM^{-1} in the area of the bronchioles (bb) area, 0.114 mGy WLM^{-1} in the area of the alveolar-interstitial (AI), and 5.78 mGy WLM^{-1} in the whole lung. The results demonstrate that when the environment was changed from the first scenario (a

typical home) to the second scenario (various factories), the doses of all regions (BB region, bb region, AI region, and whole lung) ranged from 214.29, 245.82, 3.04, and 154.38 mGy.WLM^{-1} for workers at gypsum factory to 1425.39, 1635.11, 20.26, and 1062.92 mGy.WLM^{-1}, respectively, for workers at the red brick 1 factory, and rose by a factor of 10^3, implying that one of the crucial factors determining the dose is the radon concentration. The consequences are similar to those that have been reported in the literature. In the current study, the effective dose for the lungs in the domestic setting was determined using a dosimetric approach, and the result was 13.87 mSv.WLM^{-1}, which is in the middle of the DCFs found in earlier studies. Calculations for additional anatomical, physiological, and environmental characteristics are required to broaden the current research. It will probably enhance environmental radiation protection, an issue that has recently received much attention, particularly in areas with high radon concentrations.

Ethical responsibilities of authors

All authors have read, comprehended, and cooperated, as necessary, with the Instructions for Authors' declaration on "Ethical Responsibilities of Authors."

Author contributions

All of the authors had an impact on the idea and layout of the study. [Sardar Qader Othman, Ali Hassan Ahmad, and Sarbaz Ibrahim Mohammed] assembled the materials, collected the data, and finished the analysis. Once the initial draft was completed by [Sardar Qader Othman], all contributors offered criticism on earlier versions of the work. The final draft was examined and revised by all authors.

Funding

This research received no external funding

Conflict of interest

There are no material financial or non-financial interests to disclose for the authors.

References

[1] Darby S, Hill D, Auvinen A, Barros-Dios J, Baysson H, Bochicchio F, et al. Radon in homes and risk of lung cancer: collaborative analysis of individual data from 13 European case-control studies. Br Med J 2005;330(7485):223. https://doi.org/10.1136/bmj.38308.477650.63.

[2] Monchaux G, Morlier J, Altmeyer S, Debroche M, Morin M. Influence of exposure rate on lung cancer induction in rats exposed to radon progeny. Radiat Res 1999;152(6s):S137–40. https://doi.org/10.2307/3580132.

[3] Monchaux G, Morlier J, Morin M, Chameaud J, Lafuma J, Masse R. Carcinogenic and cocarcinogenic effects of radon and radon daughters in rats. Environ Health Perspect 1994;102(1):64–73. https://doi.org/10.1289/ehp.9410264.

[4] UNSCEAR. Effects of ionizing radiation: report to the general assembly with scientific annexes, united nations scientific committee on effects of atomic radiation. New York: United Nations Publications; 2008.

[5] Fakir H, Hofmann W, Caswell RS. Radon progeny microdosimetry in human and rat bronchial airways: the effect of crossfire from the alveolar region. Radiat Protect Dosim 2008;130(2):149–61. https://doi.org/10.1093/rpd/ncm496.

[6] Hofmann W. Modelling inhaled particle deposition in the human lung—a review. J Aerosol Sci 2011;42(10):693–724. https://doi.org/10.1016/j.jaerosci.2011.05.007.

[7] Hofmann W, Winkler-Heil R. Radon lung dosimetry models. Radiat Protect Dosim 2011;145(2–3):206–12. https://doi.org/10.1093/rpd/ncr059.

[8] Harley NH, Cohen BS, Robbins ES. The variability in radon decay product bronchial dose. Environ Int 1996;22:959–64. https://doi.org/10.1016/S0160-4120(96)00208-5.

[9] Hammood H, Al-Khalifa I. Radon concentration measurement in water of Dhi–Qar Governorate (in Iraq) using emanometer. J Basrah Researches ((Sciences)) 2011;37(5). ISSN¸¸1817¸¸2695.

[10] Oufni L, Manaut N, Taj S, Manaut B. Determination of radon and thoron concentrations in different parts of some plants used in traditional medicine using nuclear track detectors. Am J Environ Protect 2013;1(2):34–40. https://doi.org/10.12691/env-1-2-4.

[11] Nain M, Chauhan R, Chakarvarti S. Alpha radioactivity in Indian cement samples. Radiat Res 2006;3(4):171–6.

[12] Sakoda A, Ishimori Y, Yamaoka K, Kataoka T, Mitsunobu F. Absorbed doses of lungs from radon retained in airway lumens of mice and rats. Radiat Environ Biophys 2013;52:389–95. https://doi.org/10.1007/s00411-013-0478-5.

[13] UNSCEAR. Sources and Effects of ionizing radiation. United nations scientific committee on effects of atomic radiation. Exposures from natural radiation sources. New York, USA: Annex B. United Nations Publication; 2000.

[14] Farkas Á, Balásházy I. Development and application of a complex numerical model and software for the computation of dose conversion factors for radon progenies. Radiat Protect Dosim 2015;164(3):278–90. https://doi.org/10.1093/rpd/ncu269.

[15] ICRP. ICRP publication 60: 1990 recommendations of the international commission on radiological protection. Pergamon Ann ICRP 1992;21(1–3):1991.

[16] ICRP. International commission on radiological protection. The 2007 recommendations of the international commission on radiological protection. ICRP Publication Ann ICRP 2007;103:2–4.

[17] ICRP. Publication 65: Protection against Radon-222 at home and work. Pergamon Press; 1993.

[18] ICRP., I. nternational Commission on Radiological Protection. Lung cancer risk from radon and progeny and statement on radon: Elsevier. 2010.

[19] Raaschou-Nielsen O, Andersen CE, Andersen HP, Gravesen P, Lind M, Schüz J, et al. Domestic radon and childhood cancer in Denmark. Epidemiology 2008:536–43. https://doi.org/10.1097/01.ede.0000288431.93533.7f.

[20] Henshaw DL, Eatough JP, Richardson RB. Radon as a causative factor in induction of myeloid leukaemia and other cancers. Lancet 1990;335(8696):1008–12. https://doi.org/10.1016/0140-6736(90)91071-H.

[21] Ishimori Y, Mitsunobu F, Yamaoka K, Tanaka H, Kataoka T, Sakoda A. Performance of the first Japanese large-scale facility for radon inhalation experiments with small animals. Radiat Protect Dosim 2011;146(1–3):31–3. https://doi.org/10.1093/rpd/ncr100.

[22] Othman SQ, Ahmed AH, Mohammed SI. Environmental health risks of radon exposure inside selected building factories in Erbil city, Iraq. Int J Environ Anal Chem 2022:1–15. https://doi.org/10.1080/03067319.2022.2107923.
[23] Schum M, Yeh H-C. Theoretical evaluation of aerosol deposition in anatomical models of mammalian lung airways. Bull Math Biol 1980;42:1–15. https://doi.org/10.1007/BF02462363.
[24] Sakoda A, Ishimori Y, Fukao K, Yamaoka K, Kataoka T, Mitsunobu F. Lung dosimetry of inhaled radon progeny in mice. Radiat Environ Biophys 2012;51:425–42. https://doi.org/10.1007/s00411-012-0431-z.
[25] ICRP. Human respiratory tract model for radiological protectionvol. 66. Pergamon, Oxford: ICRP Publication; 1994.
[26] Yeh H, Schum G, Duggan M. Anatomic models of the tracheobronchial and pulmonary regions of the rat. Anat Rec 1979;195(3):483–92. https://doi.org/10.1002/ar.1091950308.
[27] Oldham MJ, Robinson RJ. Predicted tracheobronchial and pulmonary deposition in a murine asthma model. Anat Rec: Advances in Integrative Anatomy and Evolutionary Biology: Advances in Integrative Anatomy and Evolutionary Biology 2007;290(10):1309–14. https://doi.org/10.1002/ar.20593.
[28] Zhu H, Li J, Qiu R, Pan Y, Wu Z, Li C, et al. Establishment of detailed respiratory tract model and Monte Carlo simulation of radon progeny caused dose. J Radiol Prot 2018;38(3):990. https://doi.org/10.1088/1361-6498/aac987.
[29] Beir V, Council NR. Health effects of exposure to radon. Committee on health risks of exposure to radon, Board on radiation effects research, Commission on life sciences. National Research Council; 1999.
[30] Tsuda A, Henry FS, Butler JP. Particle transport and deposition: basic physics of particle kinetics. Compr Physiol 2013;3(4):1437. https://doi.org/10.1002/cphy.c100085.
[31] Yeh H-C, Schum G. Models of human lung airways and their application to inhaled particle deposition. Bull Math Biol 1980;42(3):461–80. https://doi.org/10.1016/S0092-8240(80)80060-7.
[32] Schum M, Yeh H-C. Theoretical evaluation of aerosol deposition in anatomical models of mammalian lung airways. Bull Math Biol 1980;42(1):1–15.
[33] Wang C-S. Inhaled particles. Elsevier; 2005. eBook ISBN: 9780080455013.
[34] Asgharian B, Hofmann W, Miller F. Mucociliary clearance of insoluble particles from the tracheobronchial airways of the human lung. J Aerosol Sci 2001;32(6):817–32. https://doi.org/10.1016/S0021-8502(00)00121-X.
[35] (NCRP). National council on radiation protection and measurements. Deposition, retention and dosimetry of inhaled radioactive substances NCRP report No 125 NCRP. Bethes; 1997.
[36] Felicetti SA, Wolff RK, Muggenburg BA. Comparison of tracheal mucous transport in rats, Guinea pigs, rabbits, and dogs. J Appl Physiol 1981;51(6):1612–7. https://doi.org/10.1152/jappl.1981.51.6.1612.
[37] ICRP. Relative biological effectiveness (RBE), quality factor (Q), and radiation weighting factor (w R) ICRP Publication 92: approved by the Commission in January 2003. Ann ICRP 2003;33(4):1–121.
[38] Marsh J, Birchall A. Sensitivity analysis of the weighted equivalent lung dose per unit exposure from radon progeny. Radiat Protect Dosim 2000;87(3):167–78. https://doi.org/10.1093/oxfordjournals.rpd.a032993.
[39] Keith S, Doyle J, Harper C, Mumtaz M, Tarrago O, Wohlers D, et al. Toxicological profile for radon. Atlanta (GA): agency for toxic substances and disease registry (US). Appendix D, overview of basic radiation physics. Chemistry, and biology. Available from: https://www.ncbi.nlm.nih.gov/books/NBK158792/.
[40] Winkler-Heil R, Hussain M, Hofmann W. Stochastic rat lung dosimetry for inhaled radon progeny: a surrogate for the human lung for lung cancer risk assessment. Radiat Environ Biophys 2015;54:225–41. https://doi.org/10.1007/s00411-015-0591-8.
[41] James AC, Birchall A, Akabani G. Comparative dosimetry of BEIR VI revisited. Radiat Protect Dosim 2004;108(1):3–26. https://doi.org/10.1093/rpd/nch007.
[42] Marsh J, Birchall A, Davis K. Comparative dosimetry in homes and mines: estimation of K-factors. Elsevier Radioact Environ 2005;7:290–8. https://doi.org/10.1016/S1569-4860(04)07032-9.
[43] Nikezic D, Lau B, Stevanovic N, Yu K. Absorbed dose in target cell nuclei and dose conversion coefficient of radon progeny in the human lung. J Environ Radioact 2006;89(1):18–29. https://doi.org/10.1016/j.jenvrad.2006.03.001.
[44] Porstendörfer J. Physical parameters and dose factors of the radon and thoron decay products. Radiat Protect Dosim 2001;94(4):365–73. https://doi.org/10.1093/oxfordjournals.rpd.a006512.
[45] Comparison of modeling concepts for radon progeny lung dosimetry. ElsevierWinkler-Heil R, Hofmann W, editors. Int Congr 2002. https://doi.org/10.1016/S0531-5131(01)00506-4.
[46] UNSCEAR Ia. ICRP and UNSCEAR. Information note for participants at the IAEA TechnicalMeeting on the implications of the new dose conversion factorsfor radon, 1-4 Oct 2019. 2019. https://wwwns.iaea.org/committees/files/RASSC/1947/ICRP-UNSCEARInformationNoteonRadon.pdf (2020).
[47] UNSCEAR. Report ofthe united nations scientific committee on the effects of atomic radiation. UNSCEAR 2019 report, annex B, lung cancerfrom exposure to radon. New York: United Nations; 2020. p. 2020.
[48] ICRP. International commission ofRadiation units and measurements. Measurement andreporting ofradon exposures. ICRU report 88. J ICRU 2012;12(2):2012.
[49] Elzain A-EA. Assessment of environmental health risks due to indoor radon levels inside workplaces in Sudan. Int J Environ Anal Chem 2021:1–17. https://doi.org/10.1080/03067319.2021.1873317.